Kinetic Characterization and X-ray Structure of a Mutant of Haloalkane Dehalogenase with Higher Catalytic Activity and Modified Substrate Range[†,‡]

Joost P. Schanstra,[§] Ivo S. Ridder,[||] Gaston J. Heimeriks,[§] Rick Rink,[§] Gerrit J. Poelarends,[§] Kor H. Kalk,[||] Bauke W. Dijkstra,[||] and Dick B. Janssen*,[§]

Laboratory of Biochemistry and Laboratory of Biophysical Chemistry, BIOSON Research Institute, Groningen Biomolecular Sciences and Biotechnology Institute, University of Groningen, Nijenborgh 4, 9747 AG Groningen, The Netherlands

ABSTRACT: Conversion of halogenated aliphatics by haloalkane dehalogenase proceeds via the formation of a covalent alkyl−enzyme intermediate which is subsequently hydrolyzed by water. In the wild type enzyme, the slowest step for both 1,2-dichloroethane and 1,2-dibromoethane conversion is a unimolecular enzyme isomerization preceding rapid halide dissociation. Phenylalanine 172 is located in a helix−loop−helix structure that covers the active site cavity of the enzyme, interacts with the Cl_β of 1,2-dichloroethane during catalysis, and could be involved in stabilization of this helix−loop−helix region of the cap domain of the enzyme. To obtain more information about the role of this residue in dehalogenase function, we performed a mutational analysis of position 172 and studied the kinetics and X-ray structure of the Phe172Trp enzyme. The Phe172Trp mutant had a 10-fold higher k_{cat}/K_m for 1-chlorohexane and a 2-fold higher k_{cat} for 1,2-dibromoethane than the wild-type enzyme. The X-ray structure of the Phe172Trp enzyme showed a local conformational change in the helix−loop−helix region that covers the active site. This could explain the elevated activity for 1-chlorohexane of the Phe172Trp enzyme, since it allows this large substrate to bind more easily in the active site cavity. Pre-steady-state kinetic analysis showed that the increase in k_{cat} found for 1,2-dibromoethane conversion could be attributed to an increase in the rate of an enzyme isomerization step that preceeds halide release. The observed conformational difference between the helix−loop−helix structures of the wild-type enzyme and the faster mutant suggests that the isomerization required for halide release could be a conformational change that takes place in this region of the cap domain of the dehalogenase. It is proposed that Phe172 is involved in stabilization of the helix−loop−helix structure that covers the active site of the enzyme and creates a rigid hydrophobic cavity for small apolar halogenated alkanes.

The first step in the degradation of 1,2-dichloroethane by the bacterium *Xanthobacter autotrophicus* GJ10 is catalyzed by the enzyme haloalkane dehalogenase (Janssen et al., 1985). The enzyme converts a broad range of haloalkanes to the corresponding alcohols with water as the sole cosubstrate (Keuning et al., 1985). The protein consists of two domains (Verschueren et al., 1993a): a main domain that is formed by an eight-stranded β-sheet surrounded by α-helices, and a cap domain formed by five helices and loops. The hydrophobic active site is buried and located between these two domains. The main domain has structural similarity with several other hydrolytic enzymes, which were classified as α/β-hydrolase fold enzymes (Ollis et al., 1992).

The reaction mechanism and kinetic mechanism of haloalkane dehalogenase were deduced from X-ray crystallography, site-directed mutagenesis and pre-steady-state kinetic studies (Figure 1). The reaction is initiated by binding of 1,2-dichloroethane in the Michaelis complex, where the Cl_α of the substrate is stabilized between NH's of the Trp125 and Trp175 side chains. These two tryptophans stabilize the chloride ion when the carbon−chlorine bond is cleaved upon attack of the nucleophilic O_δ of Asp124 (Verschueren et al., 1993b,c; Pries et al., 1994a; Kennes et al., 1995). This results in the formation of a covalent alkyl−enzyme intermediate which is subsequently hydrolyzed by a water molecule activated by the general base His289 (Verschueren et al., 1993b; Pries et al., 1995a). Asp260 is hydrogen bonded to His289, which may activate the histidine by stabilizing the positive charge that develops on the imidazole ring when His289 accepts a proton from water. The slowest step at high substrate concentration is not cleavage of the carbon−halogen bond, but release of the charged halide ion out of the buried active site cavity (Schanstra & Janssen, 1996a; Schanstra et al., 1996b). In the wild type enzyme, halide release and halide binding can occur via two parallel routes. Halide release was found to follow mainly the route in which actual release of the halide ion from the enzyme was preceded by a slow unimolecular enzyme isomerization step (Schanstra & Janssen, 1996a).

The largely hydrophobic active site cavity of the dehalogenase is lined with the catalytic-triad residues Asp124, His289, and Asp260 and with four phenylalanines, two
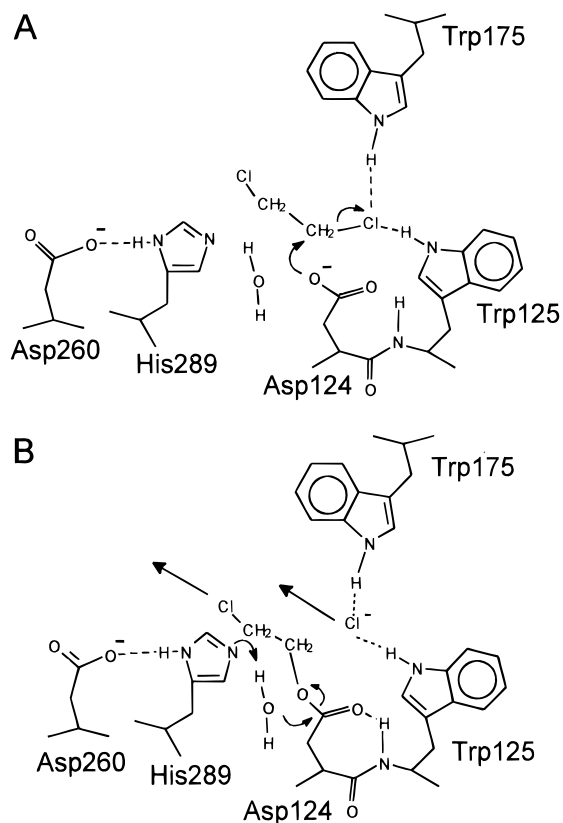

FIGURE 1: Proposed catalytic mechanism of haloalkane dehalogenase. (A) Nucleophilic attack of Asp124 on the C_α of the alkylhalide, leading to formation of the covalent alkyl−enzyme intermediate. (B) His289-assisted hydrolysis of the intermediate.

tryptophans, two leucines, a valine, and a proline (Verschueren et al., 1993a). Crystallographic studies of substrate conversion showed that Phe172 is one of the residues that interacts with the substrate during several stages of the reaction (Verschueren et al., 1993b). In the Michaelis complex, the Cl_β of the substrate is not bound very tightly and may interact with Phe128, Phe172, and perhaps Phe164. In the alkyl−enzyme, the Cl_β of the substrate lies in the plane of the Phe172 side chain and can be stabilized by interactions with the hydrogen atoms at the $C_{\delta 1}$ and $C_{\epsilon 1}$ atoms of this residue (Verschueren et al., 1993b). Furthermore, Phe172 is one of the hydrophobic residues that can be involved in stabilization of the part of the cap domain that is N-terminal of Trp175 (Pries et al., 1994b).

To evaluate the role of Phe172 in the dehalogenase reaction, we performed a random mutational analysis of this residue and studied the effects of the mutations. Pre-steady-state kinetic analysis of the Phe172Trp mutant showed that an increase in the rate of 1,2-dibromoethane conversion could be attributed to an increase in the rate of bromide release, confirming that this is the rate-determining step in the wild type enzyme. The X-ray structure of the Phe172Trp mutant suggested that this increase in the rate of halide release and also an increased affinity and conversion rate for 1-chlorohexane in this mutant could be caused by a structural change in the helix−loop−helix region formed by residues 159−181 of the cap domain of the enzyme.

MATERIALS AND METHODS

Materials. Restriction enzymes and isopropyl β-D-thiogalactopyranoside (IPTG) were obtained from Boehringer Mannheim. Bacteriophage R408, T7 polymerase, and DNA sequencing reagents were obtained from Pharmacia. Monodeoxyribonucleoside-5′-triphosphates (dNTPs) were obtained from Promega. The oligonucleotides for site-directed mutagenesis and sequencing were supplied by Eurosequence, Groningen (The Netherlands). The oligonucleotides used were pF172X (5′-AGC<u>CTGCAG</u>ATGGC**NNN**ACCGCCTG-GAAA-3′, *Pst*I restriction site underlined and mutated codon in bold) and pF172C (5′-AGC<u>CTGCAG</u>ATGGC**TGT**AC-CGCCTGG-3′, *Pst*I restriction site underlined, and mutated codon in bold). *Escherichia coli* strain BW313 (Kunkel et al., 1985) was used for the production of single-stranded uracil containing DNA used in mutagenesis. *E. coli* JM101 (Promega) was the host for production of single-stranded DNA used for sequencing and *E. coli* strain BL21(DE3) (Studier et al., 1990) was used for overexpression of both wild type and mutant dehalogenases.

DNA Methods. All DNA and *E. coli* manipulations were performed using standard molecular biology techniques described by Sambrook et al. (1989). Mutants were constructed using the method described by Kunkel et al. (1985), using vector pGELAF$^+$ (Schanstra et al., 1993). Sequences were confirmed by dideoxy sequencing (Sanger et al., 1977).

Protein Expression and Purification. Wild type and mutant enzymes were expressed and purified as described earlier (Schanstra et al., 1993). The cultures expressing the mutant enzymes were, after induction with IPTG, cultivated overnight at 17 °C to prevent inclusion body formation. The buffers used during purification were TEMAG [10 mM Tris-sulfate, pH 7.5, 1 mM EDTA, 1 mM 2-mercaptoethanol, 3 mM sodium azide, and 10% (v/v) glycerol] and PEMAG [10 mM sodium phosphate, pH 6.0, 1 mM EDTA, 1 mM 2-mercaptoethanol, 3 mM sodium azide, and 10% (v/v) glycerol]. The enzyme was concentrated with an Amicon ultrafiltration cell using a PM10 filter and stored in TEMAG-buffer at 4 °C.

Protein Analysis and Dehalogenase Assays. Protein concentrations of crude extracts were determined with Coomassie Brilliant Blue using bovine serum albumin as a standard. The concentration of purified wild type enzyme was determined using $\epsilon_{280} = 4.87 \times 10^4$ M^{-1} cm^{-1} (Schanstra & Janssen, 1996a). $\epsilon_{280} = 5.44 \times 10^4$ M^{-1} cm^{-1} was used for the Phe172Trp enzyme, and $\epsilon_{280} = 5.00 \times 10^4$ M^{-1} cm^{-1} was used for the Phe172Tyr enzyme, based on the modified protein sequences calculated with the program DNASTAR (DNASTAR Inc., Madison, WI). The purified proteins were analyzed with SDS−PAGE which showed that the purity of the preparations was greater than 99% (not shown). Dehalogenase assays were performed using colorimetric detection of halide release as described by Keuning et al. (1985). Solvent kinetic isotope effects were determined similarly with substrate dissolved in increasing concentrations of ^{2}H$_2$O. The K_m and k_{cat} were determined as described (Schanstra et al., 1996b). The experimental error in the data was less than 15% for the k_{cat} values and less than 25% for the K_m values.

Pre-Steady-State Kinetic Experiments. Rapid-quench-flow experiments were carried out at 30 °C on a rapid-quench-flow instrument (RQF-63) from KinTek Instruments (Johnson, 1992) as described by Schanstra et al. (1996b). All reported concentrations are in the reaction line of the rapid-quench-flow instrument.

Stopped-flow fluorescence was used to study the kinetics of halide binding and substrate conversion. All experiments

Scheme 1
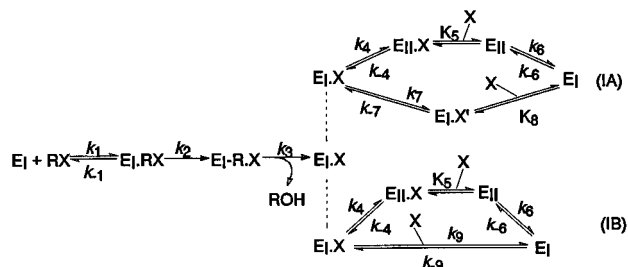
Scheme 2
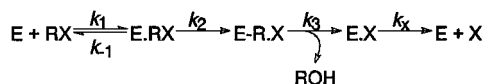
were performed on an Applied Photophysics model !SX17MV stopped-flow fluorospectrophotometer at 30 °C. Excitation was at 290 nm and fluorescence emission from Trp residues was followed through a 320 nm cutoff filter supplied with the instrument. The reported concentrations are those in the reaction chamber.

The buffer used during stopped-flow fluorescence and rapid-quench-flow experiments was $T_{50}EMA$-buffer (50 mM Tris-sulfate, pH 8.2, 1 mM EDTA, 1 mM 2-mercaptoethanol, and 3 mM sodium azide) or $T_{50}EDA$-buffer (50 mM Tris-sulfate, pH 8.2, 1 mM EDTA, 1 mM dithiothreitol, and 3 mM sodium azide). $T_{50}EDA$-buffer was used in rapid-quench experiments with 1,2-dibromoethane, since 2-mercaptoethanol interfered with 2-bromoethanol during gas chromatographic analysis. All substrate solutions were prepared in $T_{50}EMA$ or $T_{50}EDA$. Halide binding was performed in $T_{50}EMAG$ [$T_{50}EMA$-buffer with 10% (v/v) glycerol]. Glycerol was present during halide binding experiments since it improved the reproducibility of the stopped-flow fluorescence binding curves, but did not affect the kinetics.

Kinetic Data Analysis. Analysis of rapid-quench and stopped-flow fluorescence data was done by numerical simulation using the computer program Gepasi (Mendes, 1993; Gepasi for MS-Windows, version 2.0, release 2.08) coupled to the spreadsheet program Quattro-Pro 5.0 for MS-Windows (Borland International, Inc.).

The combined schemes for halide release (Schanstra & Janssen, 1996a) and substrate conversion (Schanstra et al., 1996b) by the dehalogenase are given in Scheme 1 (1A, bromide; 1B, chloride). In this scheme, E_I is the normal native enzyme, E_{II} is the kinetically observed conformational isomer to which halide ions can rapidly bind, and $E_I.X'$ is the kinetically observed collision complex in which halide is weakly bound to native enzyme (Schanstra & Janssen, 1996a). Rate and equilibrium constants for halide binding under pseudo-first-order conditions were obtained by numerical simulation of Scheme 1A and 1B as described. Apparent steady-state dissociation constants (K_d) for halide binding were determined as described by Kennes et al. (1995). Apparent dissociation constants were also calculated from the kinetic and equilibrium constants indicated in Scheme 1A and 1B (Schanstra & Janssen, 1996a).

Numerical simulation of Scheme 2, which is a simplified version of Scheme 1, was used to derive rate constants for substrate conversion. The steady-state kinetic parameters under initial velocity steady-state conditions for Scheme 2

are

$$k_{cat} = \frac{k_2 k_3 k_X}{(k_2 k_3 + k_2 k_X + k_3 k_X)},$$

$$K_m = \frac{k_3 k_X(k_{-1} + k_2)}{k_1(k_2 k_3 + k_2 k_X + k_3 k_X)},$$

and

$$\frac{k_{cat}}{K_m} = \frac{k_1 k_2}{(k_{-1} + k_2)},$$

which were derived using the method described by Huang (1979).

For clarity, the overall rate of halide release as determined from halide binding under pseudo-first-order conditions is depicted by k_{off}, whereas the rate of halide release as determined with pre-steady-state analysis of substrate conversion is depicted by k_X. The k_{off} was extracted from the rate and equilibrium constants for Scheme 1A and 1B by simulation with Gepasi. The simulation was started with all enzyme present in the form of $E_I.X$ and halide concentration zero.

Crystallization. Four mutants were subjected to crystallization experiments, Phe172Met, Phe172Trp, Phe172Tyr, and Phe172Val. Protein was dissolved in 5 mM phosphate buffer (pH 6.0), with 1 mM EDTA, 1 mM 2-mercaptoethanol, and 3 mM sodium azide. Prior to the crystallization trials, an extra purification step on a Mono Q ion-exchange column was performed, since this was shown to be essential to obtain good quality crystals of the wild type enzyme (Verschueren et al., 1993a). All experiments were performed at room temperature using the vapor diffusion method in hanging drop setups. The drops consisted of 6 μL of equal amounts of reservoir and protein solution ($\pm$5 mg of protein/mL in 100 mM MES [2-(N-morpholino)ethanesulfonic acid) buffer, pH 5.8]. Ammonium sulfate was used as a precipitant in the concentration range of 44%−58% saturation (at 0 °C), with and without 5% (v/v) PEG (polyethylene glycol) 400 as an additive, in 100 mM MES buffer, pH 5.6−6.2.

Only crystals of the Phe172Trp mutant could be grown, from 52 to 56% (w/v) saturated (at 0 °C) $(NH_4)_2SO_4$ in 100 mM MES buffer, pH 5.8. The crystals had the monoclinic space group $P2_1$, with cell parameters $a = 95.7$ Å, $b = 73.5$ Å, $c = 41.6$ Å, and $\beta = 91.3°$. These are just slightly different from the conditions and parameters for the wild type orthorhombic crystal form (Rozeboom et al., 1988). The asymmetric unit contains two molecules.

Diffraction Data Collection. A data-set was collected from one single crystal at room temperature on an Enraf Nonius FAST area detector system (Enraf Nonius, Delft, The Netherlands). The detector was equipped with a CAD4 κ-goniostat with graphite monochromatized Cu Kα radiation ($\lambda = 1.5418$ Å) from an Elliot GX21 rotating anode X-ray generator. Data were collected and processed using the MADNES package (Messerschmidt & Pflugrath, 1987). Profile fitting and local scaling of the data was done according to Kabsch (1988) and afterward merged with the in-house BIOMOL crystallographic package. Further information on the data processing is given in Table 1.

Table 1: Statistics of Data Collection and Stereochemical Quality of the Final Model

cell parameters	$a = 95.7$ Å, $b = 73.5$ Å, $c = 41.6$ Å, $\beta = 91.3°$
resolution range (Å)	35−2.67 Å
total no. of observations	43 099
no. of unique reflections	15 796
no. of discarded observations[a]	1155
R_{merge} (%)[b]	10.1% (∞−2.67 Å), 31.2% (2.77−2.67 Å)
$\langle I/\sigma(I) \rangle$	9.7 (∞−2.67 Å), 3.7 (2.77−2.67 Å)
completeness of data (%)	93.6% (∞−2.67 Å), 83.1% (2.77−2.67 Å)

Stereochemical Quality

	molecule		
	A	B	overall
rms deviations from ideality for			
bond lengths (Å)	0.012	0.012	0.012
bond angles (deg)	1.9	1.9	1.9
ΔB for bonded atoms (Å^2)	3.6	3.6	3.6
average B-factor (Å^2)	12.8	13.5	13.2
final R-factor (10−2.67 Å, all data)			20.5%
free R-factor (10−2.7 Å, 5% test set)			25.8%
estimated coordinate error (Å)[c]			0.25

[a] Intensities which deviated more than 4.5σ from the mean.

$$^b R_{\text{merge}} (\%) = \frac{\sum_{hkl}\sum_{\text{refl}} |I(hkl,j) - \bar{I}(hkl)|}{\sum_{hkl}\sum_{\text{refl}} |I(hkl,j)|}.$$

[c] Derived from a σ_A plot (Read, 1986).

Molecular Replacement and Crystallographic Refinement. The structure was solved by molecular replacement. The structure of the wild type haloalkane dehalogenase at pH 6.2 (Verschueren et al., 1993a) was used as a search model with Phe172 replaced by Ala. Self-rotation and cross-rotation functions were calculated according to Crowther (1972) with data ranging from 10 to 3.0 Å. The translation function (6.0−3.0 Å data) used was that according to Crowther and Blow (1967). The relative position of the second molecule with respect to the first molecule was found with BRUTE (Fujinaga & Read, 1987).

The model was refined with X-PLOR version 3.1 (Brünger, 1992a). A random set of five percent of the unique reflections was set apart to calculate R^{free} values (Brünger, 1992b) as an independent validation of the refinement progress. First, a rigid body refinement was done to position the two independent molecules more precisely in the asymmetric unit. In all subsequent steps, strong non-crystallographic symmetry restraints were imposed on the two molecules and only strong reflections [$F \geq 2\sigma(F)$] were used. Then two rounds of simulated annealing (4000→300 K) plus positional refinement were applied trying several values for the relative weight of the X-ray term (8.0−3.0 Å data). This cycle was repeated once with data to the resolution maximum. An OMIT $F^o - F^c$ electron density map (Bhat, 1988) calculated at this stage clearly showed density for the side chain of residues 172 in both molecules. The side chains of residues 172 were then extended to tryptophans, followed by two cycles of alternating positional and restrained individual B-factor refinement. Another cycle of positional and B-factor refinement was used to make some final corrections. At all stages OMIT $2F^o - F^c$ and $F^o - F^c$

Table 2: Activities of Wild Type and Phe172 Mutant Haloalkane Dehalogenases in Crude Extracts

mutant[a]	1,2-dichloroethane[b] (units/mg)	1,2-dibromoethane[b] (units/mg)
wild type	2.98	2.32
tryptophan	1.30	5.46
tyrosine	1.16	6.19
histidine	0.030	0.88
methionine	−[c]	1.57
glycine	−	0.040
alanine	−	0.100
valine	−	0.075
leucine[d]	−	0.040
isoleucine[d]	−	0.045
glutamate	−	0.025
asparagine	0.010	0.065
arginine	−	0.010
serine	−	0.090
threonine	−	0.010
proline	−	0.020

[a] The expression levels of soluble wild type and mutant haloalkane dehalogenases were similar (not shown). [b] Activity at 5 mM substrate. [c] −, not detectable (below 0.010 units/mg). [d] Phe172Leu and Phe172Ile haloalkane dehalogenase formed inclusion bodies at 17 °C, thus little soluble dehalogenase was produced in these two mutants.

electron density maps were calculated and inspected with O (Jones et al., 1991) to check the agreement of the model with the data. PROCHECK (Laskowski et al., 1993) was used to assess the stereochemical quality. Whenever necessary the model was manually adjusted with O. No water molecules were included. When the refinement gave no further decrease in R^{free} nor any improvement in stereochemistry, it was stopped.

RESULTS

Mutants of Phenylalanine 172. Using random site-directed mutagenesis, 15 different mutants of Phe172 were obtained (Table 2). The mutants were constructed in two mutation rounds. In the first round, inactive mutants were obtained by Kunkel mutagenesis using oligonucleotide pF172X and wild type haloalkane dehalogenase as single-stranded DNA-template. Screening for inactive mutants was done by incubating *E. coli* BL21(DE3) grown on LBi plates in 1,2-dibromoethane vapour. LBi plates are LB plates that contain bromothymol blue as a pH indicator that gives yellow instead of green/blue colonies upon production of HCl or HBr by the active dehalogenase (Schanstra et al., 1993). Inactive colonies were analyzed for the occurrence of the additional *Pst*I restriction site that was present in the mutant oligonucleotide. In the second mutation round, mutant DNA-template (Phe172Gly) obtained in the previous mutation round and encoding an inactive haloalkane dehalogenase was used to obtain mutants with activity for 1,2-dibromoethane. Screening was again done on LBi plates in *E. coli* BL21-(DE3).

Only mutant enzymes in which Phe172 was substituted by other aromatic amino acids retained an activity for 1,2-dichloroethane which was significantly above the detection limit of the assay. Furthermore, only substitution of Phe172 by Trp, Tyr, His, and Met yielded an enzyme that was active with 1,2-dibromoethane. Mutation to Trp and Tyr resulted in an increased catalytic activity with 1,2-dibromoethane. A Phe172Cys dehalogenase was constructed to see whether this mutant also retained activity with 1,2-dibromoethane. This

Table 3: Kinetic Properties of Purified Wild Type and Phe172Trp and Phe172Tyr Haloalkane Dehalogenase

substrate	property	wild type	Phe172Trp	Phe172Tyr
1,2-dibromoethane	K_m (mM)	0.010	0.025	0.12
	k_{cat} (s^{-1})	3.0	5.9	5.3
	k_{cat}/K_m (M^{-1} s^{-1})	3.0×10^5	2.4×10^5	4.4×10^4
	k_D/k_H	0.5	0.5	0.4
1,2-dichloroethane	K_m (mM)	0.53	5.13	4.96
	k_{cat} (s^{-1})	3.3	2.9	1.5
	k_{cat}/K_m (M^{-1} s^{-1})	6.2×10^3	5.6×10^2	3.0×10^2
	k_D/k_H	0.4	1	0.9
1-bromo-2-chloroethane	K_m (mM)	<0.07[a]	0.1	0.1
	k_{cat} (s^{-1})	3.2	5.5	4.8
	k_{cat}/K_m (M^{-1} s^{-1})	—	5.5×10^4	4.8×10^4
1-chlorohexane	K_m (mM)	1.4	0.57	0.90
	k_{cat} (s^{-1})	0.088	0.38	0.31
	k_{cat}/K_m (M^{-1} s^{-1})	63	6.7×10^2	3.4×10^2

[a] Lower values could not be measured due to the detection limit of 2-chloroethanol by gas chromatography.
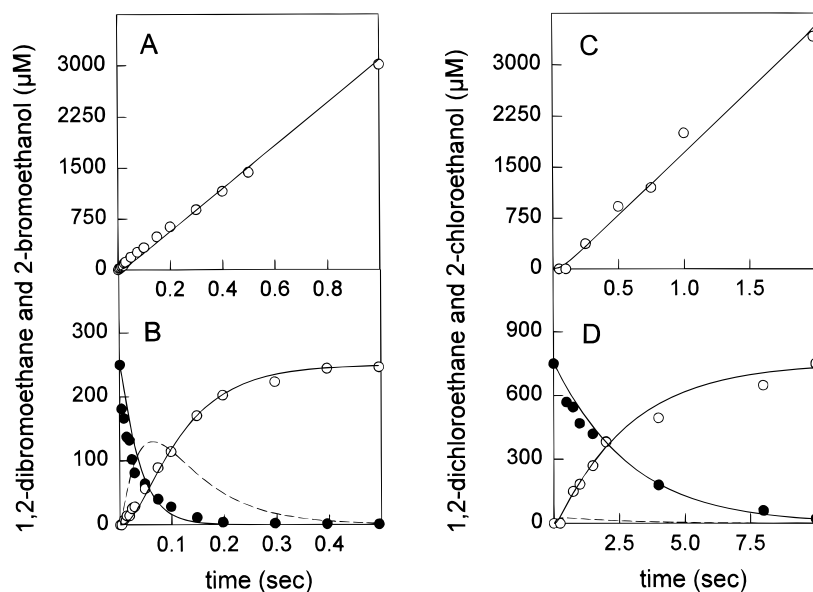

FIGURE 2: Pre-steady-state kinetic analysis of 1,2-dibromoethane and 1,2-dichloroethane conversion by Phe172Trp haloalkane dehalogenase. (A) Rapid-quench experiment with 10 mM 1,2-dibromoethane and 500 μM enzyme. The steady-state rate of alcohol production was 6 $\pm$ 0.3 s^{-1}, as determined from the slope of the plot. (B) Rapid-quench-flow experiment with enzyme (500 μM) in excess over 1,2-dibromoethane (250 μM). 2-Bromoethanol production (○) and 1,2-dibromoethane consumption (●) in time. (C) Rapid-quench experiment with 40 mM 1,2-dichloroethane and 650 μM enzyme. The rate of steady-state alcohol production was 2.8 $\pm$ 0.4 s^{-1} as determined from the last part (0.25−2 s) of the graph. (D) Rapid-quench-flow experiment with enzyme (770 μM) in excess over 1,2-dichloroethane (750 μM). 2-Chloroethanol production (○) and 1,2-dichloroethane consumption (●). In B and D, the dashed lines are the simulated concentrations of the alkyl−enzyme in time and the solid lines indicate the best fits to the data obtained by simulation of Scheme 2 using the rate and equilibrium constants in Table 4.

Phe172Cys enzyme, constructed by Kunkel mutagenesis using the Phe172Gly template, indeed showed activity with 1,2-dibromoethane (0.54 units/mg of protein in crude extract) and no detectable activity with 1,2-dichloroethane.

Steady-State Kinetic Parameters of Phe172Trp and Phe172Tyr Haloalkane Dehalogenases. The two mutants that displayed the highest activities in crude extracts, Phe172Trp and Phe172Tyr, were characterized in more detail (Table 3). The k_{cat} for 1,2-dibromoethane was increased 1.8 and 2-fold over the wild type for the Phe172Tyr and Phe172Trp enzyme, respectively. The k_{cat} for 1,2-dichloroethane was decreased in both mutants, however. The affinity for 1,2-dichloroethane and 1,2-dibromoethane decreased in both mutants, resulting in a lower k_{cat}/K_m than the wild type enzyme. There is a ^{2}H$_2$O solvent kinetic isotope effect on the k_{cat} of 1,2-dichloroethane conversion in the wild type enzyme. This originates both from an effect on halide release (Schanstra & Janssen, 1996a) and from an effect on hydrolysis of the alkyl−enzyme intermediate (Schanstra et

al., 1996b). This ^{2}H$_2$O kinetic isotope effect was not observed with the two mutant enzymes, as shown by k_D/k_H values of 0.9 and 1 (Table 3). This indicated that in the mutants the rate-limiting step had shifted to a step before hydrolysis of the alkyl−enzyme intermediate with this substrate. The slow step in conversion of 1,2-dibromoethane was most likely still located after formation of the covalent intermediate since the k_D/k_H was 0.4 and 0.5 for the Phe172Tyr and Phe172Trp enzyme, respectively, which was similar to the value found in the wild type (Table 3). The k_{cat} for conversion of 1-bromo-2-chloroethane, which was exclusively converted to 2-chloroethanol, was also elevated to rates close to the k_{cat} for 1,2-dibromoethane conversion.

The mutant enzymes showed a notable increase in the specificity constant (k_{cat}/K_m) with 1-chlorohexane to a value which was 10-fold higher for the Phe172Trp mutant and 5-fold higher for the Phe172Tyr mutant than for the wild type enzyme. The increase in k_{cat}/K_m was caused both by a higher k_{cat} and a lower K_m. For 1-chlorohexane the main

Table 4: Phe172Trp and Wild Type Haloalkane Dehalogenase Kinetic Constants[a] (Fits in Figure 2)

	k_1 $(\mu M^{-1} s^{-1})$	k_{-1} (s^{-1})	k_2 (s^{-1})	k_3 (s^{-1})	k_X (s^{-1})	$k_{cat}(calc)^b$ (s^{-1})	$K_m(calc)^b$ (μM)
1,2-dibromoethane							
wild type	0.75 ± 0.1	>20	>130	10 ± 2	4 ± 1.5	2.8	4.3
Phe172Trp	0.4 ± 0.1	25 ± 5	30 ± 5	9 ± 1.5	75 ± 25	6.3	29
1,2-dichloroethane							
wild type	$(9 \pm 1) \times 10^{-3}$	20 ± 5	50 ± 10	14 ± 3	8 ± 2	4.6	0.72×10^3
Phe172Trp	$(3 \pm 1) \times 10^{-3}$	30 ± 5	4.5 ± 1	9.5 ± 1	>75	2.9	7.5×10^3

[a] Wild-type data are from Schanstra et al. (1996b). [b] Steady-state kinetic parameters calculated from the obtained rate constants for a four-step reaction mechanism (see Materials and Methods).
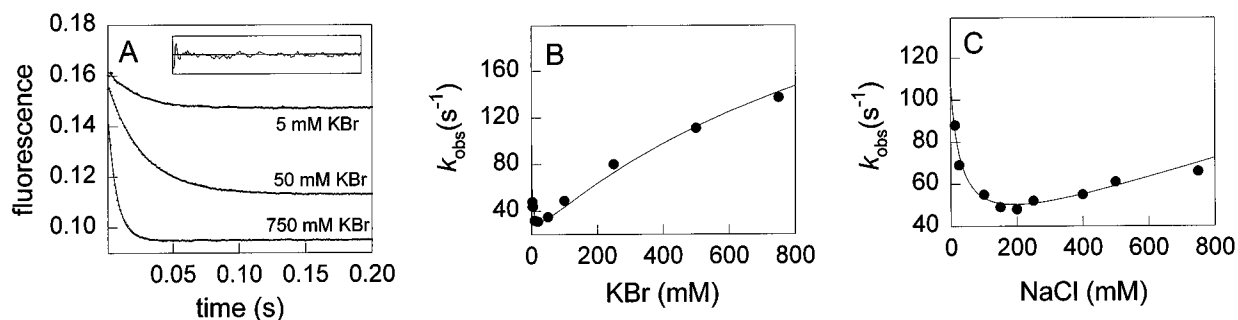

FIGURE 3: Halide binding of Phe172Trp haloalkane dehalogenase (5 μM) under pseudo-first-order conditions. (A) Three representative fluorescence transients obtained upon binding of bromide by Phe172Trp dehalogenase (5 μM). Inset, residuals from a single exponential fit to the fluorescence transient obtained with 50 mM KBr. (B) The dependence of the k_{obs} (●) obtained from single exponential fits to fluorescence transients observed at 3−750 mM KBr. (C) The dependence of the k_{obs} (●) on the chloride concentration. Values obtained from single exponential fits to fluorescence transients of chloride binding (12.5−750 mM NaCl). The solid lines are the best fits to the data obtained by numerical simulation of Scheme 1A and 1B using the rate and equilibrium constants given in Table 5.

rate-limiting step occurs before hydrolysis of the alkyl−enzyme intermediate (Schanstra et al., 1996b).

Pre-Steady-State Kinetic Analysis of 1,2-Dibromoethane Conversion. Substrate conversion by the Phe172Trp mutant was studied with pre-steady-state kinetic techniques to establish which steps in the catalytic cycle determined the altered kinetics of this mutant. A rapid-quench-flow experiment with 1,2-dibromoethane in excess over enzyme showed a nearly linear production of 2-bromoethanol in time (Figure 2A). This indicates that the rate of a step before hydrolysis of the alkyl−enzyme intermediate or the hydrolysis step itself was close to the steady-state k_{cat} (Schanstra et al., 1996b). Formation of the alkyl−enzyme intermediate was faster than its breakdown since the substrate decrease and product increase curves crossed at about 60 μM in a single-turnover experiment with 250 μM 1,2-dibromoethane and 500 μM enzyme (Figure 2B). This indicates that alkyl−enzyme accumulated and that the slowest step in the catalytic mechanism must be hydrolysis of the alkyl−enzyme intermediate.

An estimate for the rate of 1,2-dibromoethane binding (k_1) was obtained from numerical simulation of the initial 20 ms of a stopped-flow fluorescence transients obtained from a single-turnover experiment (15 μM enzyme and 15 μM 1,2-dibromoethane) and of the initial 50 ms of the transient from an experiment in which enzyme (15 μM) was mixed with 100 μM 1,2-dibromoethane (not shown). This first part of the transient is related to substrate binding (Schanstra et al., 1996b). For the simulations, the relative fluorescence of the intermediates for the quenched Phe172Trp enzyme were set 13% lower than those of the wild type enzyme (Schanstra & Janssen, 1996a), based on the assumption that the fluorescence of the additional tryptophan was also quenched. The combined experiments resulted in a k_1 of 0.4 ± 0.1 μM^{-1} s^{-1}. A similar value for k_1 (0.3 μM^{-1} s^{-1}) was obtained from

analysis of the observed rate of 1,2-dibromoethane binding (initial 50 ms) under pseudo-first-order conditions (not shown). The rate of substrate dissociation (k_{-1}) was set at the beginning of the simulation and fitting procedure to a value that was similar to or larger than that of the wild type enzyme (≥ 20 s^{-1}). This value was fine-tuned during the fitting procedure with the experimentally determined steady-state kinetic parameters as additional constraints.

Combining these data with the rapid-quench-flow data resulted in rates that can explain the kinetics of this mutant with 1,2-dibromoethane (Table 4, Scheme 2, Figure 2A and B). The slowest step in the sequence was found to be hydrolysis of the alkyl−enzyme, which had a rate constant of 9 s^{-1} and could explain the effect of ^2H_2O found on the steady-state k_{cat} (Table 3). The most important conclusion was that the rate of bromide release (k_X) was clearly higher with the Phe172Trp enzyme than with the wild type enzyme. The increase in the steady-state k_{cat} with 1,2-dibromoethane of the Phe172Trp enzyme was mainly caused by this elevated rate of halide release, which could be set at values between 50 and 100 s^{-1} without affecting the fit. The rate of carbon−bromine bond cleavage was reduced 4-fold in the Phe172Trp enzyme.

Bromide Release. The increased rate of bromide release with the Phe172Trp enzyme was confirmed by stopped-flow fluorescence experiments of bromide binding under pseudo-first-order conditions. All stopped-flow fluorescence transients obtained from mixing Phe172Trp enzyme (5 μM) with 3 to 750 mM KBr could be fitted by single exponentials (Figure 3A). The resulting dependence of the observed bromide binding rate (k_{obs}) on the bromide concentration showed that this rate decreased from 48 s^{-1} at 3 mM to around 31 s^{-1} at 30 mM KBr, followed by a hyperbolic increase of the k_{obs} at higher bromide concentrations (Figure 3B). The same dependence was found when the ionic

strength was held constant by the addition of appropriate amounts of NaF (not shown), as was also found with the wild type enzyme (Schanstra & Janssen, 1996a).

Analysis of the dependence of the k_{obs} on the bromide concentration showed that there were, as with the wild type enzyme, two parallel routes for bromide binding (Scheme 1A). Rates and equilibrium constants were extracted by simulation of Scheme 1A (Table 5) and showed that halide release mainly followed the upper route in Scheme 1A. The 11-fold increase in the overall rate of halide release (k_{off}) compared to the wild type enzyme could be attributed to an increase in the rate of the unimolecular enzyme isomerization step (k_4) that preceded the actual dissociation of halide and enzyme.

Conversion of 1,2-Dichloroethane. The absence of a solvent kinetic isotope effect on the steady-state rate of 1,2-dichloroethane conversion suggested that neither hydrolysis of the alkyl−enzyme intermediate nor halide release was rate-limiting in the Phe172Trp mutant (Table 3). Stopped-flow fluorescence analysis of chloride binding under pseudo-first-order conditions showed that the overall rate of chloride release (k_{off}) had increased to 108 s^{-1}, which was 7-fold faster than with the wild type enzyme (Table 5). This observation confirmed that chloride release cannot be rate-limiting in this mutant. The dependence of the k_{obs} on the chloride concentration, which over the complete concentration range could be fitted with single exponentials (12.5−750 mM NaCl), was similar to that of the wild type enzyme (Scheme 1B, Figure 3C).

Further information about the rates of the separate steps of 1,2-dichloroethane conversion was obtained from rapid-quench-flow experiments. An experiment with substrate in excess over enzyme showed a clear lag in 2-chloroethanol formation (Figure 2C). Thus, a step before hydrolysis of the alkyl−enzyme or hydrolysis itself was rate-limiting. In an experiment with substrate in excess over enzyme, one cannot distinguish the rates of k_2 and k_3. A single-turnover experiment with enzyme (770 μM) in excess over substrate (750 μM) showed that the substrate decrease and product increase curves crossed at 370 μM (Figure 2D), indicating that hydrolysis of the alkyl−enzyme (k_3, Scheme 2) was at least as fast as its formation. Extraction of rate constants for the reaction needed, like with 1,2-dibromoethane conversion, additional input from stopped-flow fluorescence experiments of substrate conversion (not shown). Again, an estimate of the rate of substrate binding (k_1) could be extracted from the initial part stopped-flow fluorescence transients (3 ± 1 mM^{-1} s^{-1}).

Using numerical simulation and fitting, a complete set of rate constants could be derived for 1,2-dichloroethane conversion by the Phe172Trp mutant (Table 4). The slowest step in the sequence was cleavage of the carbon-halogen bond, which was 4.5 s^{-1}. The rate of halide release (k_X) could be fitted with values larger than 75 s^{-1}, which was in agreement with the rates found in chloride binding experiments under pseudo-first-order conditions. The fact that carbon−halogen bond cleavage had become rate-limiting can explain the loss of the solvent kinetic isotope effect on 1,2-dichloroethane conversion and the decrease in steady-state k_{cat}, although the rate of chloride release, which was rate-limiting in wild type enzyme, had increased.

Structure Determination: Molecular Replacement and Crystallographic Refinement. To establish the structural

Table 5: Rates and Equilibrium Constants of Halide Binding to Phe172Trp and Wild Type Haloalkane Dehalogenase (Fits in Figure 3)[a]

	k_4 (s^{-1})	k_{-4} (s^{-1})	k_6 (s^{-1})	k_{-6} (s^{-1})	k_7 (s^{-1})	k_{-7} (s^{-1})	K_8 (mM)	k_9 (s^{-1})	k_{-9} (mM^{-1} s^{-1})	K_d(app)[b] (mM)	K_d(calc)[c] (mM)	k_{off}[d] (s^{-1})
KBr												
wild type	9 ± 1	>900	>300	3 ± 0.5	0.6 ± 0.1	110 ± 20	$(1.5 ± 0.6) × 10^3$	−[e]	−	10 ± 1	8	9.6
Phe172Trp	100 ± 30	>1 × 10^4	>1300	13 ± 2	4.5 ± 0.5	350 ± 50	$(1.3 ± 0.4) × 10^3$	−	−	16 ± 0.5	17	105
NaCl												
wild type	14.5 ± 0.5	>1450	>300	3 ± 0.3	−	−	−	0.66 ± 0.03	$(8.5 ± 0.5) × 10^{-3}$	75 ± 5	78	15
Phe172Trp	100 ± 10	>1 × 10^4	>2200	22 ± 2	−	−	−	7.5 ± 0.5	$(5.0 ± 0.5) × 10^{-2}$	150 ± 23	150	108

[a] Wild-type values were taken from Schanstra and Janssen (1996a). [b] Apparent K_d obtained from steady-state fluorescence measurements. [c] Calculated apparent steady-state K_d from obtained rate and equilibrium constants when assuming that the equilibria $E_I \leftrightarrow E_{II}$ and $E_I.X \leftrightarrow E_{II}.X$ in Scheme 1A and $E_I.X \leftrightarrow E_{II}.X$ in Scheme 1A and 1B are strongly to the left (Schanstra & Janssen, 1996a). [d] Overall halide release rates at [X] = 0 mM (see Materials and Methods). [e] −, not applicable for scheme used in fit.
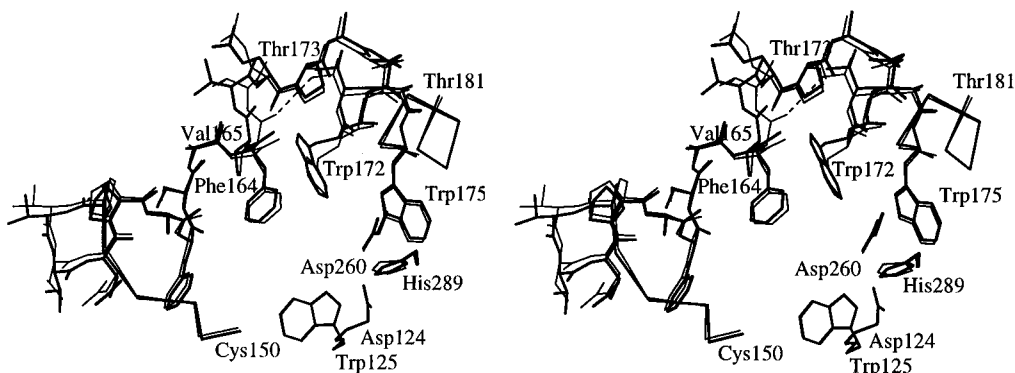
FIGURE 4: Superposition of Phe172Trp (thick lines) and wild type (thin lines) dehalogenases for the catalytic residues and residues 150−181.

basis for the observed kinetic effects we determined the X-ray structure of the Phe172Trp dehalogenase. A self-rotation function showed two peaks: the origin peak and a peak at 74% height of the origin, representing a non-crystallographic 2-fold (screw) axis in the *a,c*-plane, 1.3° off the *a*-axis. The position of the axis corresponds to the position of a 2_1-axis in the wild type crystals. A cross-rotation function yielded two peaks in the section $\beta = 90°$, which are related by the self-rotation operator. A translation function positioned the first solution of the cross-rotation function at fractional coordinates $xyz = (0.93, y', 0.71)$ and the second rotational solution at $xyz = (0.58, y'', 0.71)$. The relative position in y of the two molecules in the asymmetric unit was found to be at $\Delta y = 0.38$. This solution had a good *R*-value of 28% (correlation coefficient = 0.67).

In the course of the subsequent crystallographic refinement the model had to be adjusted only slightly. The tryptophan residues at positions 172 could be modeled nicely into difference Fourier electron density. Both the working and free *R*-factor decreased monotonically from 39.9% and 42.7% for the starting model (8−4.0 Å data) to 17.5% and 24.3%, respectively, for the final model (6.0−2.7 Å data). The final model contained two complete molecules of 310 amino acid residues per asymmetric unit and had an *R*-factor of 20.1% for all data between 10 and 2.7 Å resolution. The Ramachandran plot showed two outliers in generously allowed regions for both molecules, residues Asp124 and Asn148, and the same residues were also deviating in the wild type structure (Verschueren et al., 1993a). Some parameters indicating the stereochemical quality of the final model are given in Table 1.

Structure of Phe172Trp Enzyme. A few differences were observed between the non-crystallographically related molecules. The side chains of the surface residues Asp9 and Asp184 adopted slightly different conformations in the monomers, with χ^1/χ^2 values for Asp9 of −78°/−41° and −77°/31° in molecules A and B, respectively. No obvious structural reason was apparent, however. Asp184 had χ^1/χ^2 values of 230°/11° and 240°/138° in molecules A and B, respectively. In molecule A, Asp184O$_{\delta1}$ was hydrogen bonded to N$_{\eta2}$ of Arg186, while in molecule B Arg186 was involved in a crystal contact with Asn43. Also the average temperature factor in the N-terminal part of the cap domain (residues 155−175) was 3 Å^2 higher in molecule B, which is significantly more than the overall difference of the averages, 0.5 Å^2. In molecule A, this region was stabilized by eleven intermolecular contacts, whereas molecule B had only five contacts. Nevertheless, the orientation of the

molecules in the mutant crystal lattice and the total number of intermolecular contacts were very similar to the wild type, although some detailed interactions differed. Both monomers A and B had lost the interactions between Asn14 and symmetry-related Gln167 and between Glu41 and symmetry-related Arg193. Molecule A showed new contacts between Arg112 and a related Glu228 and from Asp212 to Lys304 and Glu308. Molecule B displayed new or extra crystal contacts between Pro19 and Tyr177, Phe20 and Tyr177, Asn43 and Arg186, and Glu72 and Ser183. These changed intermolecular contacts have been caused by the conformational change in the 165−166 region (see below).

The three-dimensional structure of the mutant was very similar to the wild type structure at pH 6.2 (Verschueren et al., 1993a). The catalytic triad, formed by residues Asp124, His289, and Asp260, was intact, and the amino acids lining the active site cavity were also in an identical orientation (Figure 4). The cavity volume as calculated with VOIDOO (Kleywegt & Jones, 1994) had not changed significantly. The tryptophan side chain introduced at position 172 was located in the same plane as the phenylalanine in wild type, with the six-membered aromatic rings in an identical position. The bigger size of the Trp172 side chain has caused the main chain of residues Val165 and Thr166 to move outward by about 1.1 Å for the Cα atoms (Figure 4). The hydrogen bond between Thr173Oγ1 and Val165O was hereby disrupted in the mutant (interatomic distance 4.7 Å vs 3.3 Å in the wild type). Due to this outward displacement, the adjacent Phe164 has also moved from its position in the wild type enzyme by about 0.5 Å, thus weakening the quadrupole−quadrupole interaction between the aromatic rings at positions 164 and 172.

DISCUSSION

Phenylalanine 172 of haloalkane dehalogenase interacts with the Cl$_\beta$ and C$_\alpha$ of 1,2-dichloroethane in the Michaelis complex and alkyl−enzyme during catalysis (Verschueren et al., 1993b), and therefore it might affect the mode of binding and reaction rate of this substrate. Furthermore, inspection of the structure indicates that Phe172 may be involved in stabilization of the N-terminal helix−loop−helix region between residue 159 and 181 of the cap domain by the stabilizing interactions between Phe172 and Phe164. To obtain information about the role of phenylalanine 172 in haloalkane dehalogenase structure and function, we performed a mutational analysis of position 172, and studied the X-ray structure and steady-state and pre-steady-state kinetics of the Phe172Trp enzyme.

Inspection of the X-ray structure of the Phe172Trp dehalogenase showed that the two tryptophans that make up the halide binding site of the enzyme (Verschueren et al., 1993c) were at the same positions in the Phe172Trp mutant as in the wild type enzyme (Figure 4). The bigger size of the Trp side chain compared to wild type Phe had forced the main chain atoms of residues Val165 and Thr166 to move outward (Figure 4), causing the loss of the Thr173Oγ1- - -Val165O hydrogen bond. Because of the displacement of the main chain at positions 165 and 166, the packing interactions made in wild type by the adjacent residues Gln167 and Pro168 are not present in the mutant crystals. This change has caused the mutant enzyme to crystallize in a different space group than the wild type, which forms crystals in space group $P2_12_12$ exclusively.

The catalytic properties of the Phe172Trp enzyme were significantly different from those of the wild type enzyme. The k_{cat} for 1,2-dibromoethane was about 2-fold higher for the Phe172Trp dehalogenase than for the wild type enzyme. Pre-steady-state analysis showed that this could be attributed to the increased rate of bromide release. The rate of 1,2-dibromoethane binding and C−Br bond cleavage was lower in the Phe172Trp enzyme than in the wild type enzyme, however.

The helix−loop−helix region of the cap domain of the dehalogenase contributes to the hydrophobic substrate binding site of the enzyme (Verschueren et al., 1993a,b) and it is likely that the observed conformational difference might influence the binding energy of smaller substrates such as 1,2-dichloroethane and 1,2-dibromoethane. Furthermore, the lower rate of carbon−halogen bond cleavage found in the Phe172Trp enzyme indicates that this part of the cap could also be involved in transition state stabilization during carbon−halogen bond cleavage.

For the longer substrate 1-chlorohexane, however, this structural change in the mutant seems to be favorable. 1-Chlorohexane is a poor substrate for the wild type dehalogenase (Pries et al., 1994b), and the rate-limiting step for conversion of this substrate is before hydrolysis of the alkyl−enzyme intermediate (Schanstra et al., 1996b). How this substrate is bound is unknown since the active site cavity of both the wild type dehalogenase (Verschueren et al., 1993b) and the Phe172Trp enzyme is too small to bind 1-chlorohexane, but it is conceivable that a more flexible hydrophobic active site cavity in the Phe172Trp enzyme might facilitate a conformational change to accommodate a larger substrate. Dehalogenase mutants with improved conversion of 1-chlorohexane were also obtained using *in vivo* selection (Pries et al., 1994b). No X-ray structures have been obtained for these mutants so far, but most of the changes in these mutants were located in the helix−loop−helix region of the cap domain, indicating similar changes in the active sites of these mutants as in the Phe172Trp dehalogenase.

The fact that only the Phe172Trp and the Phe172Tyr enzymes retained their activity with 1,2-dichloroethane could indicate that besides a more nonspecific hydrophobic interaction, an aromatic (172)−chlorine interaction contributes to substrate binding and transition state stabilization during C−Cl bond cleavage. This is supported by the observation that in the alkyl−enzyme of the wild type dehalogenase the Cl$_\beta$ of the 1,2-dichloroethane lies in the plane of the positively charged edge (C$_{\epsilon 1}$ and C$_{\delta 1}$) of Phe172 (Ver-

schueren et al., 1993b). The interaction of negatively charged groups with aromatic rings has also been observed with sulfur−aromatic (Reid et al., 1985; Burley & Petsko, 1988) and oxygen-aromatic interactions (Thomas et al., 1982; Burley & Petsko, 1988), where the negatively charged oxygen or sulfur exhibits affinity toward the positively charged edge of the aromatic ring.

An interaction between the enzyme and the alkyl group of the substrate seems to be less important for the dehalogenase reaction with 1,2-dibromoethane, since the Phe172Met, the Phe172Cys, and the Phe172His enzymes which were inactive with 1,2-dichloroethane had a significant activity with 1,2-dibromoethane. The difference between 1,2-dichloroethane and 1,2-dibromoethane conversion can originate from the fact that bromine is a better leaving group in S$_N$2 type reactions. Furthermore, the larger van der Waals volume of 1,2-dibromoethane compared to 1,2-dichloroethane could also lead to a more "tight" fit of this substrate in the active site cavity.

Both for 1,2-dichloroethane and 1,2-dibromoethane conversion, the rate of hydrolysis of the alkyl−enzyme intermediate in the Phe172Trp enzyme did not change significantly compared to the wild type enzyme. This is not surprising, since residues involved in this step, i.e., the Asp260−His289 couple which activates the nucleophilic water molecule and residues that form the oxyanion hole (Verschueren et al., 1993b; Pries et al., 1995a), are located in the main domain of the dehalogenase and were at nearly identical positions in the Phe172Trp and wild type enzyme.

A possible explanation for the lack of activity displayed by the other mutants in Table 2 is that the structural integrity of the active site is lost by their mutations. There was, for example, a very low affinity for bromide and chloride in the Phe172Val enzyme (J.P. Schanstra, unpublished results), while the apparent affinity constant (K_d) increased only 2-fold for the Phe172Trp enzyme (Table 5). The origin of this may be located in the loss or weakening of the interaction between residues 164 (helix 4) and 172 (helix 5) upon mutation of residue 172. In the wild type enzyme, the positively charged edge of Phe164 approaches the negative face of Phe172 (ring centroids are 5.8 Å apart and oriented perpendicular). These two residues might serve as an hydrophobic anchor for the helix−loop−helix structure, and such aromatic interactions in the interior of proteins are known to contribute to protein stability (Burley & Petsko, 1985, 1988; Hunter et al., 1991; Anderson et al., 1993). In the Phe172Trp enzyme, an interaction between these two residues is still present, and also in the Phe172Tyr, Phe172Met, Phe172Cys, and Phe172His enzymes an interaction between position 172 and 164 can be envisaged. It is known that sulfur-containing residues can interact with aromatic residues (Reid et al., 1985; Burley & Petsko, 1988). Histidine is also capable of interacting favorably with aromatic rings (Loewenthal et al., 1992; Armstrong et al., 1993; Jasanoff & Weiss, 1993). The other amino acids introduced at position 172 could either be not capable of a specific interaction with aromatic residues such as Phe164 (Gly/Ala/Val/Leu/Ile) or are likely to be too hydrophilic (Glu/Asn/Ser/Thr), disturbing the hydrophobic character of the active site cavity.

Both in the wild type enzyme (Schanstra & Janssen, 1996a) and in the Phe172Trp enzyme, we have found two routes for release of the charged halide ion out of the buried active site cavity (Scheme 1A and 1B). For the route which

is kinetically most important, actual release was preceded by a slow enzyme isomerization. Pre-steady-state kinetic analysis of halide binding under pseudo-first-order conditions showed that the overall increase in the rate of halide release in the Phe172Trp enzyme was caused by an increased rate of this unimolecular enzyme isomerization. For the wild type enzyme we have hypothesized that this enzyme isomerization could be a conformational change which is necessary to allow water to enter the active site and solvate the halide ion (Schanstra & Janssen, 1996a). The X-ray structure of the Phe172Trp enzyme showed that the two tryptophan residues between which the halogen moiety of the substrate and halide is bound were at identical positions in mutant and wild type enzyme (Figure 4), indicating that altered positions of these tryptophans were not responsible for the large difference in rate of halide release. However, the structural changes in the helix−loop−helix region that covers the active site of the dehalogenase and the observation that the rate of halide release was increased dramatically in the Phe172Trp enzyme indicates that the proposed slow conformational change necessary for solvation of the halide is located in this region. Other mutations that influence the stability of the helix−loop−helix region without affecting active site residues should indicate whether this is indeed the site of the conformational change that was identified by kinetic measurements.

REFERENCES

Anderson, D. E., Hurley, J. H., Nicholson, H. Baase, W. A., & Matthews, B. W. (1993) *Protein Sci. 2*, 1285−1290.

Armstrong, K. M., Fairman, R., & Baldwin, R. L. (1993) *J. Mol. Biol. 230,* 284−291.

Bhat, T. N. (1988) *J. Appl. Crystallogr. 21*, 279−281.

Brünger, A. T. (1992a) X-PLOR Version 3.1 Manual, Yale University, New Haven, CT.

Brünger, A. T. (1992b) *Nature 355*, 472−475.

Burley, S. K., & Petsko, G. A. (1985) *Science 229*, 23−28.

Burley, S. K., & Petsko, G. A. (1988) *Adv. Protein Chem. 39*, 125−192

Crowther, R. A. (1972) in *The Molecular Replacement Method* (Rossmann, M. G., Ed.) pp 173−178, Gordon & Breach, New York.

Crowther, R. A., & Blow, D. M. (1967) *Acta Crystallogr. 23*, 544−548.

Fujinaga, M., & Read, R. J. (1987) *J. Appl. Crystallogr. 20*, 517−521.

Huang, C. Y. (1979) *Methods Enzymol. 63*, 54−83.

Hunter, C. A., Singh, J., & Thornton, J. M. (1991) *J. Mol. Biol. 218*, 837−846.

Janssen, D. B., Scheper, A., Dijkhuizen, L., & Witholt, B. (1985) *Appl. Environ. Microbiol. 49*, 673−677.

Jasanoff, A., & Weiss, M. A. (1993) *Biochemistry 32*, 1423−1432.

Johnson, K. A. (1992) *The Enzymes 20*, 1−61.

Jones, T. A., Zou, J.-Y., Cowan, S. W., & Kjeldgaard, M. (1991) *Acta Crystallogr. A47*, 110−119.

Kabsch, W. (1988) *J. Appl. Crystallogr. 21*, 916−924.

Kennes, C., Pries, F., Krooshof, G. H., Bokma, E., Kingma, J., & Janssen, D. B. (1995) *Eur. J. Biochem. 228*, 403−407.

Keuning, S., Janssen, D. B., & Witholt, B. (1985) *J. Bacteriol. 163*, 635−

Kleywegt, G. J., & Jones, T. A. (1994) *Acta Crystallogr. D50*, 178−185.

Kunkel, T. A. (1985) *Proc. Natl. Acad. Sci. U.S.A. 82*, 488−492.

Laskowski, R. A., MacArthur, M. W., Moss, D. S., & Thornton, J. M. (1993) *J. Appl. Crystallogr. 26*, 283−291.

Loewenthal, R., Sancho, J., & Fersht, A. R. (1992) *J. Mol. Biol. 224*, 759−770.

Mendes, P. (1993) *Comput. Appl. Biosci. 9*, 563−571.

Messerschmidt, A., & Pflugrath, J. W. (1987) *J. Appl. Crystallogr. 20*, 306−315.

Ollis, D. L., Cheah, E., Cygler, M., Dijkstra, B. W., Frolow, F., Franken, S. M., Haral, M., Remington, S. J., Silman, I., Schrag, J., Sussman, J. L., Verschueren, K. H. G., & Goldman, A. (1992) *Protein Eng. 5*, 197−211.

Pries, F., Kingma, J., Pentenga, M., van Pouderoyen, G., Jeronimus-Stratingh, C. M., Bruins, A. P., & Janssen, D. B. (1994a) *Biochemistry 33*, 1242−1247.

Pries, F., van den Wijngaard, A. J., Bos, R., Pentenga, M., & Janssen D. B. (1994b) *J. Biol. Chem. 269*, 17490−17494.

Pries, F., Kingma, J., Krooshof, G. H., Jeronimus-Stratingh, C. M., Bruins, A. P., & Janssen, D. B. (1995) *J. Biol. Chem. 270*, 10405−10411.

Read, R. J. (1986) *Acta Crystallogr. A42*, 140−149.

Reid, K. S. C., Lindley, P. F., & Thornton, J. M. (1985) *FEBS Lett. 190*, 209−213.

Rozeboom, H. J., Kingma, J., Janssen, D. B., & Dijkstra, B. W. (1988) *J. Mol. Biol. 200*, 611−612.

Sambrook, J., Fritsch, E. F., & Maniatis, T. (1989) in *Molecular Cloning: A Laboratory Manual*, Cold Spring Harbor Laboratory Press, Plainview, NY.

Sanger, F., Nicklen, S., & Coulsen, A. R. (1977) *Proc. Natl. Acad. Sci. U.S.A. 74*, 5463−5467.

Schanstra, J. P., Rink, R., Pries, F., & Janssen, D. B. (1993) *Protein Exp. Purif. 4*, 479−489.

Schanstra, J. P., & Janssen, D. B. (1996a) *Biochemistry, 35*, 5624−5632.

Schanstra, J. P., Kingma, J., & Janssen, D. B. (1996b) *J. Biol. Chem. 271*, 14747−14753.

Studier, F. W., Rosenberg, A. H., Dunn, J. J., & Dubendorff, J. W. (1990) *Methods Enzymol. 185*, 60−89.

Thomas, K. A., Smith, G. M., Thomas, T. B., & Feldmann, R. J. (1982) *Proc. Natl. Acad. Sci. U.S.A. 79*, 4843−4847.

Verschueren, K. H. G., Franken, S. M., Rozeboom, H. J., Kalk, K. H., & Dijkstra, B. W. (1993a) *J. Mol. Biol. 232*, 856−872.

Verschueren, K. H. G., Seljée, F., Rozeboom, H. J., Kalk, K. H., & Dijkstra, B. W. (1993b) *Nature 363*, 693−698.

Verschueren, K. H. G., Kingma, J., Rozeboom, H. J., Kalk, K. H., Janssen, D. B., & Dijkstra, B. W. (1993c) *Biochemistry 32*, 9031−9037.